THE JOURNAL OF PHYSICAL CHEMISTRY C

ARTICLE

pubs.acs.org/JPCC

Chemical Imaging and Distribution Analysis of Mono-, Bi-, and Tridentate Alkanethiol Self-Assembled Monolayers on Gold by Sum Frequency Generation Imaging Microscopy

Marjorie Hernandez, Pawilai Chinwangso, Katherine Cimatu, La-ongnuan Srisombat, T. Randall Lee,* and Steven Baldelli*

Department of Chemistry, University of Houston, Houston, Texas 77204-5003, United States

ABSTRACT: Sum frequency generation (SFG) microscopy was used to investigate the structure and orientation of multidentate alkanethiolate monolayers on gold surfaces. Adsorbate molecules in which one, two, or three sulfur atoms coordinated to the surface of gold afforded self-assembled monolayers (SAMs) with controlled spacing between the alkyl chains. SFG imaging was used to determine the orientation of the molecules on the surface and to visualize spatial variations across the surface. Using SFG imaging, the average orientation of the terminal methyl group is measured as well as the standard deviation. Further, the presence of film defects is measured by the CH_2/CH_3 intensity ratio and the distribution quantified through the standard deviation. The results demonstrate that the tridentate adsorbate forms a monolayer in which the alkyl chains are highly disordered on the surface when compared to SAMs derived from normal alkanethiols (i.e., monodentate adsorbates). The results are consistent with a model in which the tridentate alkanethiols generate SAMs with lower alkyl chain density. SFG microscopy provides a detailed view of the origin of the monolayer disorder by statistical spectroscopic analysis of the surface.

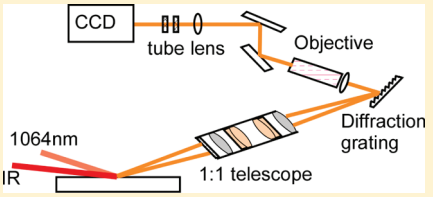

INTRODUCTION

Self-assembled monolayers (SAMs) offer well-controlled and structurally ordered surfaces that can be used in a variety of studies and applications, including adhesion, wetting, corrosion inhibition, and lubrication.[1] SAMs have also been widely investigated and used in biological systems, optical systems, nanoelectronics, information storage, and the fabrication of biosensors.[1−3] To determine the chemical and physical properties of SAMs (e.g., thickness, roughness, molecular structure, and chemical composition), the monolayers have been characterized by a variety of techniques, such as ellipsometry, contact angle goniometry, spectroscopy (electronic and vibrational), and imaging.[4−7]

One of the more revealing techniques used to characterize SAMs is sum frequency generation imaging microscopy (SFGIM).[8−10] This technique can be used to provide the chemical identification and distribution of the adsorbed molecules on the substrates. This paper examines the chemical properties of multidentate alkanethiolate SAMs in terms of packing density, distribution, and conformational order using mapping analysis with SFGIM.

Three types of alkanethiolate SAMs with different alkyl-to-sulfur atomic ratios (Figure 1) were analyzed to explore the influence of the degree of chelation on monolayer structure.

Self-assembled monolayers (SAMs) consist of ordered molecular assemblies by chemisorption of molecule on a substrate.[11] To vary the properties of SAMs, the substrate can be changed and/or the adsorbate molecules can be chemically modified for a desired application or study. For the latter, one can vary the nature of the headgroup and/or tailgroup of the molecule before deposition. Moreover, one can also study the reaction or response of the monolayers by exposing the chemisorbed monolayers to selected reagents or reaction conditions.[12] The preparation conditions can also be modified by changing the temperature, solvent, and duration of deposition.

Recently, nonlinear optical imaging has become a useful technique in the analysis of SAMs. In particular, second-harmonic generation (SHG) has been effectively used in studies of biological molecules.[13−19] SHG microscopy is a far field imaging method and a second-order nonlinear spectroscopy, which makes it a surface-sensitive technique; however, it provides electronic structure information on the interface, which is not always easy to interpret without specific labeling or any initially surface-active system. Coherent anti-Stokes Raman spectroscopy (CARS)[20−24] is also useful in providing spatially resolved vibrational spectra of the system, but being a third-order nonlinear process, CARS is not an interface-specific technique. More recently, sum frequency generation imaging microscopy (SFGIM) has been developed and used for imaging solution-deposited and patterned SAMs. This technique is advantageous because it is a vibrational spectroscopy, where external labeling is not required to achieve sensitivity, and it is inherently surface specific.[8−10,25−29]

Received: November 23, 2010
Revised: February 5, 2011
Published: February 25, 2011

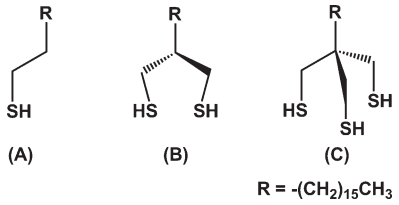

Figure 1. Structures of the chelating alkanethiols: (A) *n*-octadecanethiol (monodentate), (B) 2-monohexadecylpropane-1,3-dithiol (bidentate), and (C) 1,1,1-tris(mercaptomethyl)hexadecane (tridentate).

Sum frequency generation (SFG) is a vibrational spectroscopy involving a second-order nonlinear process; therefore, it is a surface-sensitive and viable technique for the characterization of monolayer films.[30,31] The technique involves the overlapping of two pulsed laser beams at the surface—a fixed visible beam and a tunable infrared beam. The overlap creates a third beam with a frequency that is the sum of the two input frequencies. When the IR beam matches a resonance of a specific vibrational mode of an interfacial molecule, the SFG intensity, I_{SFG}, is enhanced.[32] As shown in eq 1,

$$I_{SF} \propto \left| \sum_{JK} \chi_{IJK}^{(2)} E_J(\omega_{vis}) E_K(\omega_{IR}) \right|^2 \quad (1)$$

the intensity of the SFG signal is related to the second-order nonlinear susceptibility, $\chi_{IJK}^{(2)}$, and the amplitude of the incident beams, $E_j(\omega_{IR})$ and $E_k(\omega_{vis})$. The susceptibility $\chi^{(2)}$ is a third rank tensor that contains information regarding interfacial properties (eq 2).

$$\chi^{(2)} = \chi_R^{(2)} + \chi_{NR}^{(2)} = \sum_q \frac{A_q}{\omega_{IR} - \omega_q + i\Gamma} + \chi_{NR}^{(2)} \quad (2)$$

The tensor is the summation of resonant ($\chi_R^{(2)}$) and nonresonant susceptibilities ($\chi_{NR}^{(2)}$). The nonresonant susceptibility ($\chi_{NR}^{(2)}$) arises from the substrate (in this study, gold), while the resonant susceptibility ($\chi_R^{(2)}$) contains vibrational information of the interfacial molecules (the SAMs).[30]

In eq 2, ω_{IR} is the corresponding IR frequency, ω_q is the vibrational resonant frequencies of the qth vibrational mode, and Γ is the damping factor. The A_q term contains information regarding the infrared and Raman transition moments.

$$\chi_R^{(2)} \propto N\langle\beta^{(2)}\rangle \quad (3)$$

Thus, χ_R is proportional to the number of molecules (N) and the orientational averaged hyperpolarizability ($\beta^{(2)}$), which is the product of infrared and Raman transition moments.[30,31,33,34] The average, $\langle\rangle$, is often assumed to be a delta-function or Gaussian function of various widths. The vibrational spectrum of the surface molecules is derived by plotting the SFG intensity as a function of IR wavelength.

The efficient collection of the SFG photon signals is expected because SFG is directional due to its unique phase-matching conditions. To achieve an efficient phase matching condition, the proper phase relationship between the interacting waves for optimum nonlinear conversion must be maintained along the propagation direction. In relation to imaging, this condition is also responsible for lateral resolution, since the SFG beam, which contains all the details of a surface, is directional; therefore, a differentiation between the features on the surface can be spatially resolved.[35−37]

The SFG microscope is capable of characterizing an interface of a specific sample such as a SAM on gold by determining the chemical composition, contrast/phase transition, and resolution. It is able to determine both the spatial and chemical nature of the molecules on the surface and thus represents an excellent technique for the chemical imaging of surfaces, where averaging the signal of the whole sample is not sufficient to reveal detailed structural *and* orientational properties.[9,28]

A major goal of this study is to establish a quantitative link between the statistical image analysis of SFG microscopy and the classical average interpretation of the SAMs by techniques such as contact angle. Here a correspondence is made between the standard deviation of the measured distributions and the disorder on the film as established by previous ensemble average methods.

EXPERIMENTAL SECTION

Materials. *n*-Octadecanethiol (monodentate) was purchased from Sigma-Aldrich and used as received. The 2-monohexadecylpropane-1,3-dithiol (bidentate) and 1,1,1-tris(mercaptomethyl)heptadecane (tridentate) adsorbates were synthesized by known methods; the experimental details and complete characterization of the molecules can be found elsewhere.[38,39] Gold shot was obtained from Americana Precious Metals (99.99%). The solvent used to prepare SAMs from the monodentate and bidentate alkanethiols was absolute ethanol from Aaper, while dimethyl sulfoxide (DMSO) from Sigma-Aldrich was used to prepare the tridentate SAM.[39]

Gold Film Preparation. Si(100) wafers were precleaned with absolute ethanol prior to coating with a 10-nm chromium adhesion layer. A 100 nm gold film was then evaporated onto the substrate.

Growth SAMs on Gold. The gold substrates were immersed in a 1-mM solution of the indicated adsorbate molecule for the formation of the monolayers. After equilibration for 18 h, the SAM-coated substrate was washed with ethanol to remove any physisorbed molecules and impurities. The sample was blown dry with a stream of N_2 gas before characterization.

Laser System and SFG Microscope Setup. The laser used was a picosecond pulsed Nd:YAG laser (Ekspla) with a 20 Hz repetition rate.[40] It generates a fundamental 1064 nm beam that pumps an optical parametric generator/amplifier (OPG/OPA) manufactured by LaserVision. This parametric system can generate a tunable infrared (IR) beam from 2000 to 4000 cm^{-1}. The fundamental 1064 nm and tunable IR beams were used to generate the SFG signal from the surface. The schematic diagram of the microscope is shown in Figure 2, where the incident angles of the tunable IR and the 1064 nm beams were 70.0° and 60.0° from the surface normal, respectively. Both beams were overlapped at the same time and spaced to generate the SFG signal. The SFG signal was calculated and detected at 62.1°. Both of the incident beams were set at *p*-polarization.[8,25] The current microscope design has a spatial resolution of 2 μm.

Data Collection, Processing, and Mapping Analysis. The data were collected by continuously scanning the IR at a fixed scan rate and averaging the SFG signal over a range of 5 cm^{-1} interval with 5000 shots per data point (wavelength). At a certain region-of-interest (ROI) and specific wavelength, the pixels were averaged to acquire spectral data, and Origin 7.0 was used to plot and fit the peaks of the spectra. Spectra were curve-fitted using the Lorentzian peak function for the analysis of peak amplitude, wavenumber, and width, according to eq 2.

In the mapping analysis, a local ROI of 25 × 25 μm^2 pixel area over 825 × 825 μm^2 pixel entire image area was used. The SFG data points in each of the 25 × 25 μm^2 pixel area were extracted using a macro program plug-in with ImageJ software.[41] Each spectrum was plotted and fitted to a Lorentzian fit function. Each spectrum is normalized to the 2980 cm^{-1} wavelenth, as this is the position of highest intensity. This is important since the laser beam has a Gaussian intensity profile which makes the center of the image approximately 30% higher in intensity than the edges. Since only peak ratios are used in the spectral analysis, this method allows for comparison between the various ROI. The intensity ratios of the CH_3 asymmetric (asym)/CH_3 symmetric (sym) vibrational stretches were used for the tilt angle analysis[34,42] and the ratios of CH_2(sym)/CH_3(sym) were used for the gauche defect analysis.[30,43,44] These values were re-mapped onto the surface to provide two-dimensional contour plots that show the spatial distribution of the intensity ratios. Also, the ratio values were plotted to provide a histogram of

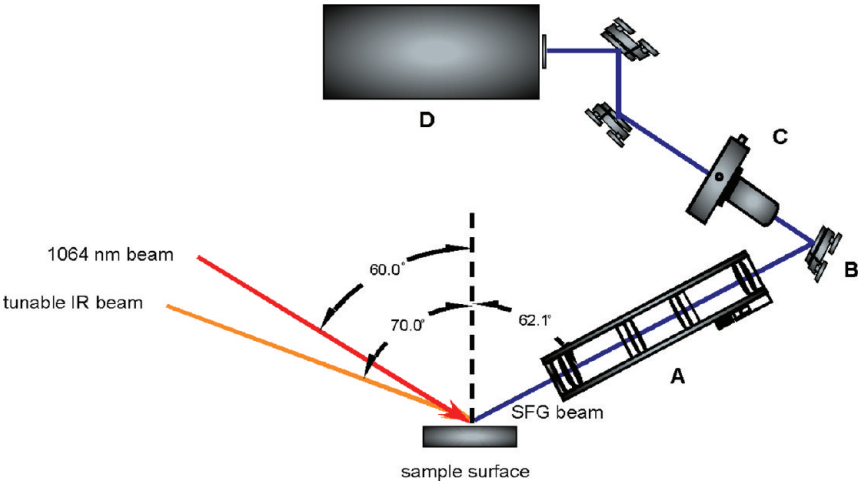

Figure 2. SFG imaging microscope setup showing the angles of incident of IR and 1064 nm beam and the angle of SFG signal generated. The following are the corresponding microscope parts: (A) 1:1 telescope, (B) diffraction grating, (C) microscope system, and (D) CCD camera detector.

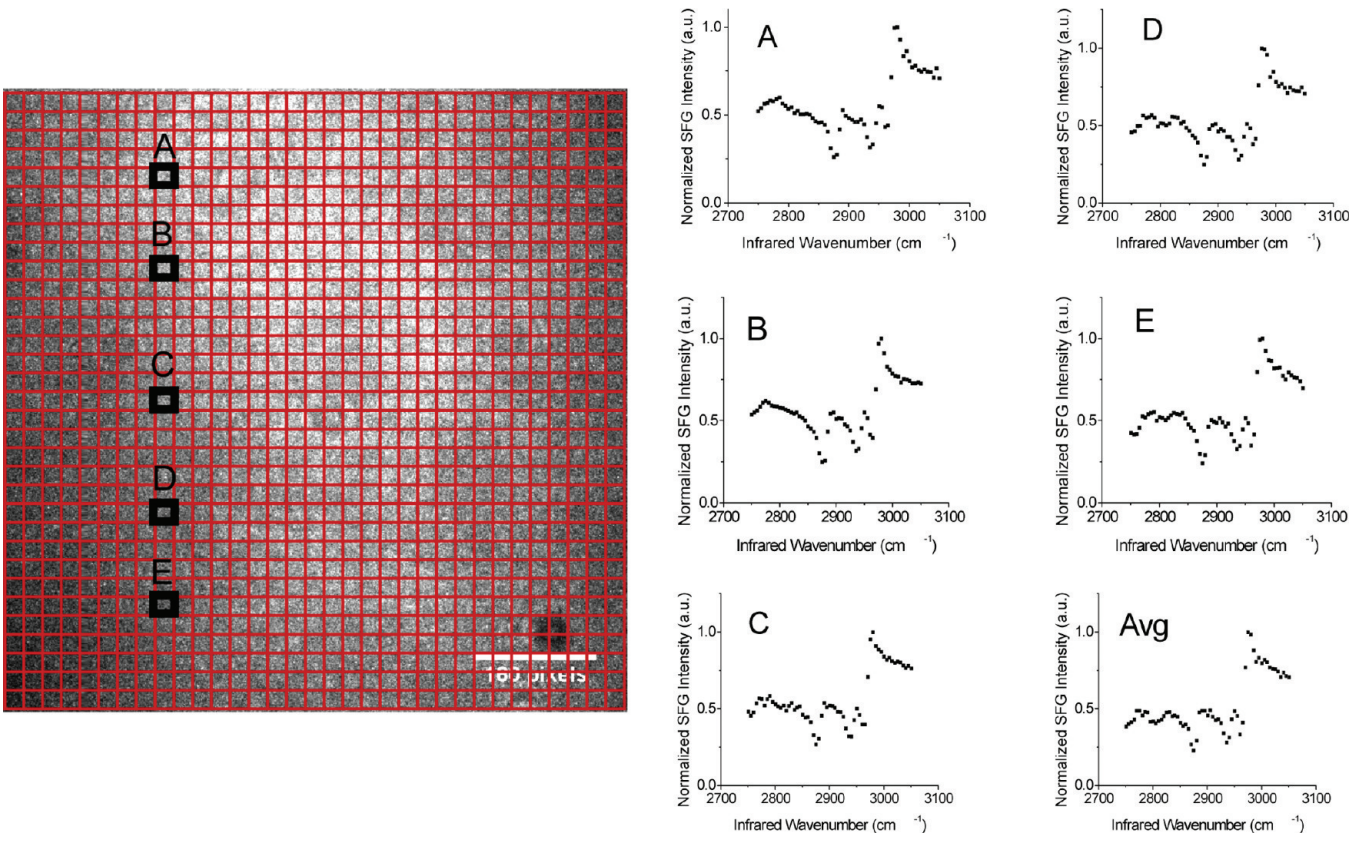

Figure 3. Spectra of stack images of 25 × 25 μm^2 pixel area at different portions of the 825 × 825 μm^2 pixel area image: A−E shows the spectra at different area. The average spectrum is also shown in Avg. This is the image obtained from monodentate alkanethiol SAM.

distribution analysis, which reveals the number of counts/occurrences or population of the specific intensity ratio.

RESULTS AND DISCUSSION

Figure 3 shows a representative 825 × 825 μm^2 pixel area image of the monodentate SAM, which was divided into a 25 × 25 μm^2 pixel area (1 pixel = 1 μm), giving a total of 1089 regions. From Figure 3b−f, the spectra vary from region to region and also show a difference from the spatially averaged spectrum, as shown in Figure 3a.

The vibrational peaks observed for all of the SAMs at 2875, 2938, and 2967 cm^{-1} correspond to the terminal methyl (CH_3) symmetric stretch, Fermi resonance, and CH_3 asymmetric stretch, respectively. For the methylene group (CH_2), the symmetric stretching and Fermi resonance [or CH_2(asym) since the assignment is not firmly assigned] stretching peaks are positioned at 2850 and ~2915 cm^{-1}, respectively, as shown in the spectrum (Figure 4). These vibrational stretches are assumed to arise from gauche defects in the alkyl chains.[45] An additional peak at 2904 cm^{-1} is also assigned to the Fermi resonance of the CH_2 symmetric stretch.[30,45−47]

Increasing the number of terminal sulfur atoms per alkyl chain of the adsorbate molecules in SAMs is expected to result in the formation of SAMs with lower packing density on the gold surface. The lower chain density corresponds to a larger interchain spacing, decreasing the van der Waals interactions, giving rise to films with diminished conformational order. Further, the increased space between the chains permits greater degrees of freedom for the alkyl chain conformation and tilt angles.

SFG spectra are used to estimate both the tilt orientation of the terminal CH_3 group relative to the surface normal and the chain conformation. The tilt angle of the methyl group is evaluated by the relative intensity of the symmetric and asymmetric peaks. In addition to the average tilt angle, the distribution of tilt angle can be inferred from the SFG images. Likewise, the conformational order of the SAMs can be evaluated using two criteria. First, the presence and magnitude of gauche defects is reflected qualitatively by the appearance of the CH_2 modes. Second, the magnitude of the disorder is reflected by the distribution width of these modes, relative to the CH_3(sym) peak, that is, the standard deviation of the CH_2/CH_3 ratio. Thus, a relationship between the spectroscopic evaluation and the nonspectroscopic methods such as ellipsometry and contact angle in the SAMs can be made.[38,39]

Methyl Group Peak Analysis. For the tilt angle analysis, the ratio of the CH_3(sym)/CH_3(asym) was used. A calculated tilt angle vs intensity ratio curve is presented in Figure 5 and was calculated on the basis of the CH_3 hyperpolarizability values and the geometry of the SFG spectrometer.[9,34] The curve assumes a delta-function distribution for the tilt angles, where all of the molecules on the surface possess the same tilt angle. In the analysis presented here, each region of interest was assigned an orientation based on this function; subsequently all the ROI were analyzed to provide the distribution of orientations on the surface. Figure 6a−c provides the contour plots and the corresponding distribution of ratios, which are presented as histograms (Figure 6d−f).

To visualize the lateral distribution of orientations of molecules, the calculated ratios values were remapped onto the two-dimensional contour plots shown in Figure 6a−c. Qualitatively, the monodentate SAM appears to be smoother, indicating a more homogeneous monolayer.

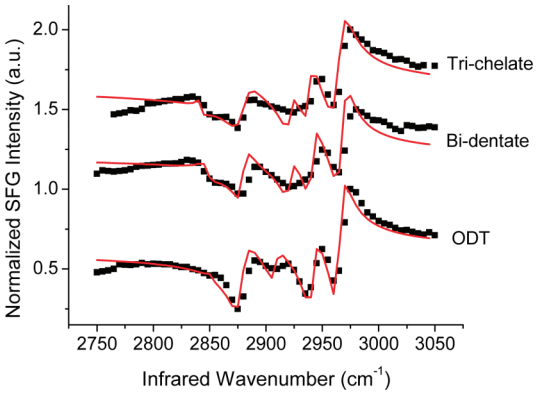

Figure 4. Average spectra acquired from bottom to top the monodentate, bidentate (offset by 0.5 units), and tridentate (offset by 1.0 units) SAMs on gold substrates. Lines are curve fits to eq 2.

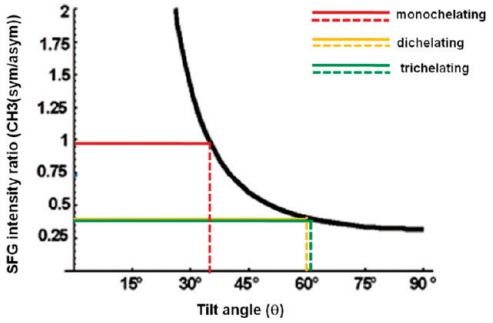

Figure 5. Orientation analysis of the average SFG using delta-function analysis. The approximate tilt angle based on the ratio for mono-, bi-, and tridentate SAMs are shown.

The histograms in Figure 6d−f which show the number of occurrences (counts) of the ratios were determined and fitted to a Gaussian distribution function to approximate the average and standard deviation (see Table 1). These values were used to determine the average tilt angle of the methyl group from the surface normal. From the histogram plots of mono-, bi-, and tridentate monolayers in Figure 6d−f, the tilt angles of the terminal methyl groups were obtained by relating the averages of the CH_3(sym/asym) ratios with the SFG theoretical curve (Figure 5). In the case of the monodentate SAM, the average ratio was determined to be 0.85, which corresponds to the tilt angle of ~38° from the surface normal. For the bidentate and tridentate SAMs, their average ratios were determined to be 0.36 and 0.32, which correspond to the approximate tilt angles of ~60° and ~62°, respectively. For these latter SAMs, their average tilt angles are almost indistinguishable. However, each SAM shows distinct distributions of the tilt angle, as determined by the width of the fitted Gaussian function. On the basis of the data in Table 1, the system that possesses the highest standard deviation and shows the greatest surface heterogeneity is the tridentate SAM. Thus, on the basis of the analysis CH_3 groups, the tridentate SAM has the greatest range of orientations, >30°.

Compared to the SAMs derived from the monodentate adsorbate, the alkyl chains of the SAMs derived from the multidentate adsorbates are expected to tilt more from the surface normal due to the void space between the chains. On the basis of

dx.doi.org/10.1021/jp1111795 |J. Phys. Chem. C 2011, 115, 4688–4695

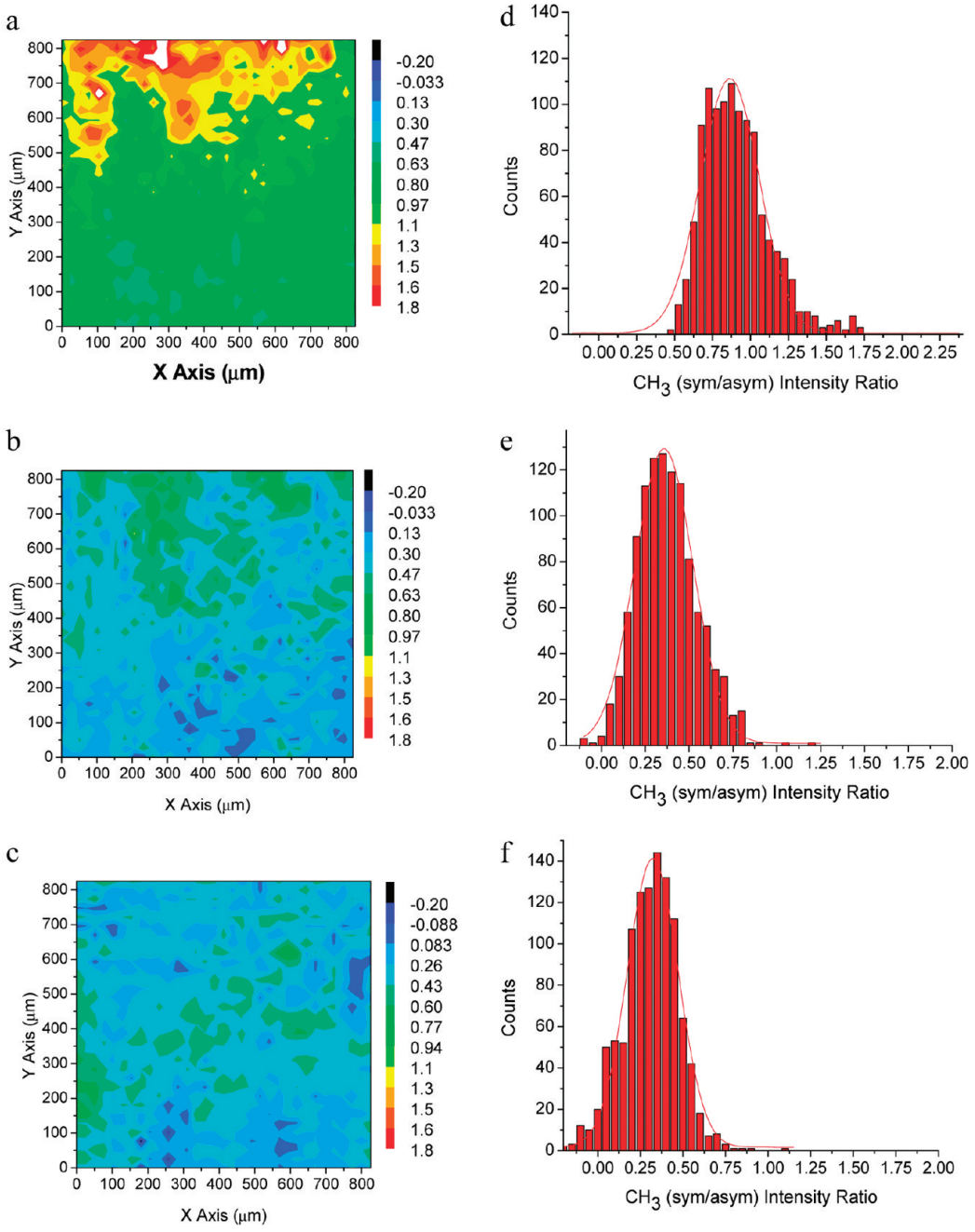

Figure 6. SFG imaging analysis of the three SAMs. Contour plots of CH_3(sym/asym) ratio of (a) monodentate, (b) bidentate, and (c) tridentate SAMs with their corresponding histogram plots (d, e, f, respectively) are shown.

Table 1. Summary of Distribution Data Obtain for Methyl Peaks of SAMs on Gold

			tilt angle (deg)	
molecule	average ratio	SD	average	range
monodentate	0.85	0.26	38	~7
bidentate	0.36	0.21	60	~20
tridentate	0.32	0.30	62	≥30

the ellipsometric data obtained by Park et al., on the identical SAMs examined here,[48] loosely packed SAMs exhibited lower thicknesses than the densely packed ones. The SFG results reinforce this finding but are based on the direct statistical analysis on the spectra of the terminal methyl groups.

Methylene Group Peak Analysis. The degree of film order was resolved using SFGIM mapping analysis of the methylene peaks and compared to the formation and quality of the normal alkanethiolate SAM (i.e., the monodentate SAM), which known to form a densely packed and well-ordered monolayer.[49,50] To visualize the surface heterogeneity, the ratios of the CH_2(sym)/CH_3(sym) were mapped as shown in Figure 7a−c, which indicates that the surface heterogeneity increases as follows: monodentate < bidentate < tridentate. Correspondingly, the

dx.doi.org/10.1021/jp1111795 |J. Phys. Chem. C 2011, 115, 4688–4695

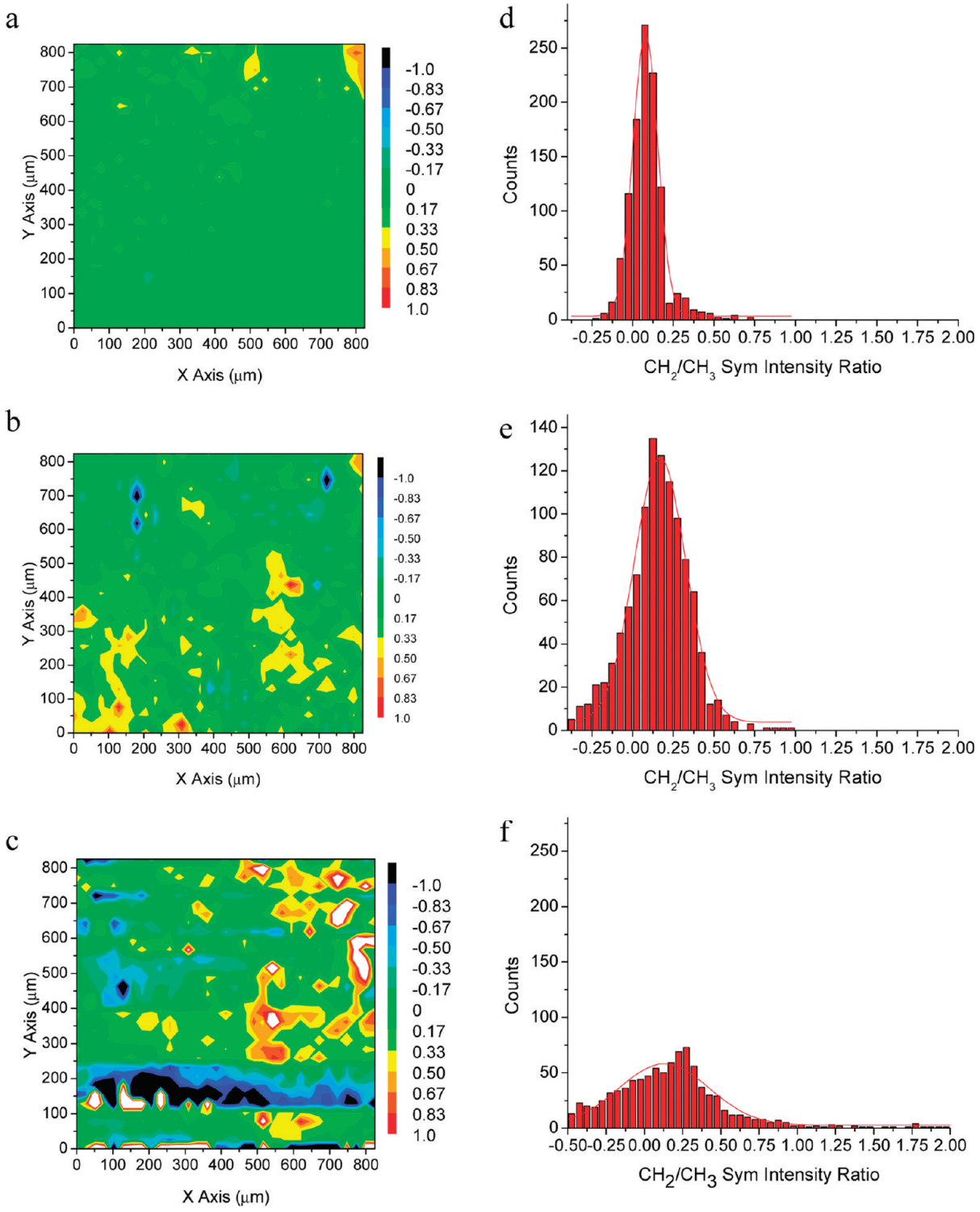

Figure 7. SFG imaging analysis of the three chelating self-assembled monolayer. Contour plots of CH_2/CH_3 symmetric stretch ratio for (a) monodentate, (b) bidentate, and (c) tridentate with their corresponding histogram plots (d, e, f), respectively.

histograms in Figure 7d−f show that the bidentate and tridentate SAMs possess greater gauche defects [as indicated by their larger ratio of $CH_2(sym)/CH_3(sym)$ peaks] when compared to the monodentate SAM. The $CH_2(sym)/CH_3(sym)$ ratio was also used to estimate the packing density of the alkyl chains on the surface. If the alkyl chains are arranged in an all-trans configuration, then the adsorbed molecules are assumed to be highly ordered and densly packed.[51] If, however, the chains deviate from this configuration, then gauche defects would be introduced to the monolayer; accordingly, CH_2 stretching modes would appear in the SFG spectra due to the loss of centrosymmetry between the CH_2 groups along the alkyl

dx.doi.org/10.1021/jp1111795 |J. Phys. Chem. C 2011, 115, 4688–4695

Table 2. Summary of Distribution Data for Methylene Peaks Obtain for SAMs on Gold

molecule	average ratio	SD
monodentate	0.08	0.15
bidentate	0.16	0.32
tridentate	0.13	0.58

chain.[30,43,44] Figure 7d−f shows the gauche defect analysis, where the histogram plots of the CH_2(sym)/CH_3(sym) ratios from each adsorbate are compared.

The data obtained from the measurements illustrated in Figure 7 are summarized in Table 2. The average ratio obtained from the tridentate SAM deviates the most from zero (i.e., highest standard deviation: 0.58) followed by the bidentate and monodentate SAMs, respectively. The larger deviation from a value of zero value represents a greater abundance of conformational defects.

Previous studies have shown that the presence of CH_2 groups at an interface causes the monolayer to be more wettable than the surface containing interfacial CH_3 groups.[39] Densely packed and well-ordered alkanethiolate SAMs on gold expose predominantly methyl groups on the surface, while SAMs that are less densely packed and less conformationally ordered expose a higher percentage of methylene groups on the surface.[49,52,53] Park et al.[48] reported the trend of the hexadecane contact angle and the conformational order of the SAMs as follows: monodentate > bidentate > tridentate SAMs. This trend suggests that the multidentate surface contains more CH_2 groups and is thus less conformationally ordered than the monodentate surface. The SFGIM mapping analysis is consistent with this interpretation, where the distribution width of the terminal methyl group orientation and the magnitude of the CH_2(sym)/CH_3(sym) ratio for the SAM follow the trend tridentate > bidentate ≫ monodentate.

Finally, SFG imaging analysis has an additional benefit; by only considering the average SFG signal, the local regions on the surface with lower order tend not to be counted in the average values, due to their lower signals. The SFG imaging has the capability of showing the detailed and important information of the SAMs on local regions of the metal surface and can be more properly accounted for in these surfaces with lower orientation and conformational order. If only the average spectrum of the entire image is considered, the well-oriented molecules in certain regions dominate the signal and can lead to a misinterpretation of the surface chemistry.

CONCLUSIONS

This paper used SFG to examine the molecular conformation of SAMs on gold derived from alkanethiols in which the alkyl−sulfur ratio was varied systematically. Variations in adsorbate structure led to defined differences in packing density and conformational order of the SAMs. Statistical analysis of the SFG images allowed for the direct evaluation of the quality of the SAMs based on distributions (i.e., the range of angles and conformations adopted by the alkyl chains). The studies indicate that the packing density and conformational order of the SAMs as deduced by SFG imaging analysis decreased as monodentate > bidentate > tridentate and is consistent with other studies performed previously.

AUTHOR INFORMATION

Corresponding Author

*E-mail: sbaldelli@uh.edu (S.B.) or trlee@uh.edu (T.R.L.). Phone: 713-743-2701. Fax: 713-743-2709.

ACKNOWLEDGMENT

We thank the National Science Foundation (DMR-0856009) and the Robert A. Welch Foundation (Grant No. E-1320) for providing generous support for this project.

REFERENCES

(1) Gorton, L.; Ed. *Comprehensive Analytical Chemistry Volume XLIV: Biosensors and Modern Biospecific Analytical Techniques*; Elsevier Science: New York, 2005.
(2) Mizutani, F. *Sens. Actuators, B* **2008**, *B130*, 14–20.
(3) Xia, Y.; Whitesides, G. M. *Annu. Rev. Mater. Sci.* **1998**, *28*, 153–184.
(4) Xia, Y.; Whitesides, G. M. *Angew. Chem., Int. Ed.* **1998**, *37*, 550.
(5) Parikh, A. N.; Nuzzo, R. G. *J. Am. Chem. Soc.* **1991**, *113*, 7152–7167.
(6) Bain, C. D.; Whitesides, G. M. *Adv. Mater.* **1989**, 1.
(7) Delamarche, E.; Michel, B.; Gerber, C.; Anselmetti, D.; Guentherodt, H. J.; Wolf, H.; Ringsdorf, H. *Langmuir* **1994**, *10*, 2869–2871.
(8) Cimatu, K.; Baldelli, S. *J. Phys. Chem. B* **2006**, *110*, 1807–1813.
(9) Cimatu, K.; Baldelli, S. *J. Phys. Chem. C* **2007**, *111*, 7137–7143.
(10) Cimatu, K.; Moore, H. J.; Barriet, D.; Chinwangso, P.; Lee, T. R.; Baldelli, S. *J. Phys. Chem. C* **2008**, *112*, 14529–14537.
(11) Ulman, A. *Chem. Rev.* **1996**, *96*, 1533.
(12) Li, J.; Thiara, P. S.; Mrksich, M. *Langmuir* **2007**, *23*, 11826–11835.
(13) Cernusca, M.; Hofer, M.; Reider, G. A. *J. Opt. Soc. Am. B* **1998**, *15*, 2476.
(14) Florsheimer, M.; Raduge, C.; Salmen, H.; Bosch, M.; Terbrack, R.; Fuchs, H. *Thin Solid Films* **1996**, *284−285*, 659.
(15) Florsheimer, M.; Bosch, M.; Brillert, C.; Wierschem, M.; Fuchs, H. *Adv. Mater.* **1997**, *9*, 1061.
(16) Florsheimer, M. *Phys. Status Solidi A* **1999**, *173*, 15.
(17) Reider, G. A.; Cernusca, M.; Hofer, M *Appl. Phys. B: Laser Opt.* **1999**, *68*, 343.
(18) Smilowitz, L.; Jia, Q. X.; Yang, X.; Li, D. Q.; McBranch, D.; Buelow, S. J.; Robinson, J. M. *J. Appl. Phys.* **1997**, *81*, 2051.
(19) Florsheimer, M.; Bosch, M.; Brillert, C.; Wierschem, M.; Fuchs, H. *J. Vac. Sci. Technol. B* **1997**, *15*, 1564.
(20) Potma, E. O.; Xie, X. S.; Muntean, L.; Preusser, J.; Jones, D.; Ye, J.; Leone, S. R.; Hinsberg, W. D.; Schade, W. *J. Phys. Chem. B* **2004**, *108*, 1296.
(21) Zumbusch, A.; Holtom, G. R.; Xie, X. S. *Phys. Rev. Lett.* **1999**, *82*, 4142.
(22) Cheng, J.-x.; Volkmer, A.; Book, L. D.; Xie, X. S. *J. Phys . Chem. B* **2001**, *105*, 1277.
(23) Cheng, J.-X.; Xie, X. S. *J. Phys. Chem. B* **2004**, *108*, 827.
(24) Cheng, J.-x.; Volkmer, A.; Book, L. D.; Xie, X. S. *J. Phys. Chem. B* **2002**, *106*, 8493.
(25) Hoffmann, D. M.; Kuhnke, K.; Kern, K. *Rev. Sci. Instrum.* **2002**, *73*, 3221.
(26) Kuhnke, K.; Hoffmann, D. M.; Wu, X. C.; Bittner, A. M.; Kern, K. *Appl. Phys. Lett.* **2003**, *83*, 3830.
(27) Cimatu, K.; Baldelli, S. *J. Am. Chem. Soc.* **2006**, *128*, 16016–16017.
(28) Cimatu, K.; Baldelli, S. *J. Am. Chem. Soc.* **2008**, *130*, 8030–8037.
(29) Cimatu, K.; Moore, H. J.; Lee, T. R.; Baldelli, S. *J. Phys. Chem. C* **2007**, *111*, 11751–11755.
(30) Bain, C. D. *J. Chem. Soc. Faraday Trans.* **1995**, *91*, 1281–96.
(31) Buck, M.; Himmelhaus, M. *J. Vac. Sci. Technol. A* **2001**, *19*, 2717–2736.
(32) Baldelli, S. *J. Phys. Chem. B* **2003**, *107*, 6148–6152.
(33) Lambert, A. G.; Davies, P. B.; Neivandt, D. J. *Appl. Spectrosc. Rev.* **2005**, *40*, 103–145.
(34) Wang, H.-F.; Gan, W.; Lu, R.; Rao, Y.; Wu, B.-H. *Int. Rev. Phys. Chem.* **2005**, *24*, 191–256.

(35) Gan, W.; Wu, B.-h.; Zhang, Z.; Guo, Y.; Wang, H.-f. *J. Phys. Chem. C* **2007**, *111*, 8716–8725.
(36) Wang, H.-F.; Gan, W.; Lu, R.; Rao, Y.; Wu, B.-H. *Int. Rev. in Phys. Chem.* **2005**, *24*, 191–256.
(37) Zheng, D.-S.; Wang, Y.; Liu, A.-A.; Wang, H.-F. *Int. Rev. Phys. Chem.* **2008**, *27*, 629–664.
(38) Shon, Y.-S.; Colorado, R.; Williams, C. T.; Bain, C. D.; Lee, T. R. *Langmuir* **2000**, *16*, 541.
(39) Park, J.-S.; Vo, A. N.; Barriet, D.; Shon, Y.-S.; Lee, T. R. *Langmuir* **2005**, *21*, 2902.
(40) Baldelli, S. *J. Phys. Chem. B* **2003**, *107*, 6148.
(41) available at http://rsb.info.nih.gov/ij, developed by Wayne Rasband, National Institutes of Health, Bethesda, MD.
(42) Hirose, C.; Yamamoto, H.; Akamatsu, N.; Domen, K. *J. Phys. Chem.* **1993**, *97*, 10064–10069.
(43) Potterton, E. A.; Bain, C. D. *J. Electroanal. Chem.* **1996**, *409*, 109–114.
(44) Miranda, P. B.; Shen, Y. R. *J. Phys. Chem. B* **1999**, *103*, 3292–3307.
(45) Snyder, R. G.; Strauss, H. L.; Elliger, C. A. *J. Phys. Chem.* **1982**, *86*, 5145–50.
(46) Duffy, D. C.; Davies, P. B.; Bain, C. D. *J. Phys. Chem.* **1995**, *99*, 15241–6.
(47) Macphail, R. A.; Strauss, H. L.; Snyder, R. G.; Elliger, C. A. *J. Phys. Chem.* **1984**, *88*, 334–341.
(48) Park, J.-S.; Vo, A. N.; Barriet, D.; Shon, Y.-S.; Lee, T. R. *Langmuir* **2005**, *21*, 2902–2911.
(49) Bain, C. D.; Troughton, E. B.; Tao, Y. T.; Evall, J.; Whitesides, G. M.; Nuzzo, R. G. *J. Am. Chem. Soc.* **1989**, *111*, 321–335.
(50) Nuzzo, R. G.; Allara, D. L. *J. Am. Chem. Soc.* **1983**, *105*, 4481–4483.
(51) Hunt, J. H.; Guyot-Sionnest, P.; Shen, Y. R. *Chem. Phys. Lett.* **1987**, *133*, 189–192.
(52) Chaudhury, M. K. *Mater. Sci. Eng. R* **1996**, *16*, 97–159.
(53) Shon, Y.-S.; Lee, S.; Colorado, R., Jr.; Perry, S. S.; Lee, T. R. *J. Am. Chem. Soc.* **2000**, *122*, 7556–7563.